



ELSEVIER

Journal of Chromatography A, 694 (1995) 15–37

JOURNAL OF
CHROMATOGRAPHY A

Review

Theoretical studies of type II–V chiral stationary phases

Kenny B. Lipkowitz

Department of Chemistry, Indiana University–Purdue University Indianapolis, Indianapolis, IN 46202-3274, USA

Abstract

A review of atomic-level molecular modeling in chiral chromatography is given. The focus of this review is on non-brush-like stationary phases with emphasis on cyclodextrin and cellulosic stationary phases. Most of the theoretical papers reviewed invoke regression models to understand where and how chiral discrimination takes place.

Contents

1. Introduction	15
2. Molecular modeling	16
2.1. Quantum mechanics (QM)	17
2.2. Molecular mechanics (MM)	17
2.3. Molecular dynamics (MD)	17
2.4. Monte Carlo simulations (MC)	17
2.5. Molecular graphics	17
3. Type II CSPs	18
4. Type III CSPs	26
5. Type IV CSPs	32
6. Type V CSPs	33
7. Summary and conclusions	36
Acknowledgement	36
References	36

1. Introduction

Separation scientists have long been interested in resolving enantiomers without having to prepare diastereomers as intermediates. This concept of direct enantiomer separation by using chiral mobile or stationary phases has, until recently, eluded the separation scientist. During the last decade, however, advances in both the science and technology of direct enantiomer

resolution have been made, and one can now routinely separate a wide range of enantiomers [1–9]. Understanding where and how chiral selection takes place in chromatography is important because it allows one to design improved chromatographic systems and it addresses fundamental concepts in chiral recognition for disciplines outside separation science. Although the intermolecular forces (hydrogen bonding, multipolar association, dispersion forces, charge-

transfer complexation, hydrophobic association, etc.) have been thoroughly studied and are well documented, precisely how these forces work in concert to promote binding is not clear. Indeed, a major effort made by research scientists in the past decade has been in the area of molecular recognition, where the goals have been to sort out how substrates bind to natural and non-natural receptors [10]. One of the difficulties in understanding how chiral recognition takes place is that the forces responsible for one enantiomer binding to a chiral surface are the same as those for its optical antipode. What one would like to have, then, is a method that allows us not only to determine which forces are at play, but also to quantitate them so that differences between mirror image isomers can be assessed. One approach that shows promise in this regard is computational chemistry [11].

In this paper, we review computational approaches that have been applied toward understanding where and how chiral recognition takes place on type II–V chiral stationary phases (CSPs). This is a follow-up to a previous review on the molecular modeling done on type I or brush-type chiral stationary phases [12]. Wainer [13] categorizes existing HPLC CSPs as follows:

Type I. Where the solute–CSP complexes are formed by attractive interactions, hydrogen bonding, π – π interactions, dipole stacking, etc., between the solute and CSP.

Type II. Where the primary mechanism for the formation of the solute–CSP complex is through attractive interactions, but where inclusion complexes also play an important role.

Type III. Where the solute enters into chiral cavities within the CSP to form inclusion complexes.

Type IV. Where the solute is part of a diastereomeric metal complex (chiral ligand-exchange chromatography).

Type V. Where the CSP is a protein and the solute–CSP complexes are based on combinations of hydrophobic and polar interactions.

The major difference between the first three categories, irrespective of the type of intermolecular attractions, is the extent of inclusion. Type I has no inclusion complexation, type II

has partial inclusion and type III uses as the “primary mechanism” inclusion complexation. For this review, a greater line of demarcation between type II and type III CSPs is created by considering type III to be exclusively guest–host complexes as found in crown ethers, cyclodextrins and related systems, whereas type II uses only partial guest–host complexation. Hence, whereas Wainer considers polymethacrylate polymers and microcrystalline cellulose triacetate as type III CSPs, we shall consider them as type II along with the other cellulose-based CSPs.

2. Molecular modeling

A model is a representation of reality. It is a likeness or a semblance, and means different things to different people. There are two categories of chemical models: macroscopic and microscopic. Macroscopic models describe coarse-grain features of a system or process. They consider, e.g., relative rates of uptake, kinetics of transport and rates of depletion of entities involved in a process without consideration of structural features of the individual molecules. Microscopic models, sometimes called atomistic models, usually take full account of all the atoms in the system.

Microscopic, atomistic modeling is done in two ways: using fitting procedures or applying theory. The fitting procedures are an attempt to rationalize connections between molecular structure and physico-chemical properties (quantitative structure–property relationships, QSPR) or with biological response (quantitative structure–activity relationships, QSAR). Usually the response is regressed onto a set of molecular descriptors, e.g., $\log(1/C) = b_0 + \sum_i b_i D_i$, where C is the concentration of a compound needed to elicit a response, b_0 is a constant, b_i are the least-squares multiple regression coefficients and D_i are molecular descriptors. One can very accurately predict an unknown molecule's property or anticipated response by computing its molecular descriptors and substituting those values into the model. There are no rules about what kind of descriptors are to be used, but

descriptors often include information about molecular size and shape, electronic effects and lipophilicity. This type of modeling requires the use of existing data to create the model and then allows one to interpolate or extrapolate new properties/activities of as yet unknown molecules within that same class of compounds. QSARs and QSPRs have been a major influence on the design of drugs and materials.

The second kind of atomistic, molecular modeling applies theory. The major tools implemented are as follows.

2.1. Quantum mechanics (QM)

The objective of quantum mechanics is to describe the spatial positions of electrons and nuclei. Most commonly implemented is the molecular orbital theory (MOT), where electrons are allowed to flow around fixed nuclei until they reach a self-consistent field (SCF). This is where the attractive and repulsive forces of all particles are in a steady state. The nuclei are iteratively moved followed by SCF calculations until the energy can go no lower. This is called energy minimization or geometry optimization and allows one to predict structural and electronic features of molecules.

2.2. Molecular mechanics (MM)

Molecular mechanics is a non-quantum mechanical method of computing structures, energies and some properties of molecules. Molecular mechanics uses an empirical force field (EFF), which is a recipe for reproducing a molecule's potential energy surface (the location and motion of nuclei on such surfaces dictate a molecule's structure and dynamic properties). A molecule is viewed as a collection of particles (nuclei) held together by elastic forces (electrons). These forces are defined in terms of potential energy functions of internal coordinates such as bond lengths, bond angles and torsion angles. Once all the potential functions and associated force constants have been determined, the internal energy is minimized by moving the particles toward their equilibrium

positions (geometry optimization). Since EFFs treat electrons implicitly rather than explicitly, molecular mechanics is much faster than quantum mechanics.

2.3. Molecular dynamics (MD)

In molecular dynamics the motion of atoms is described by Newtonian laws: $F_i(t) = m_i a_i = m_i \partial^2 r_i(t) / \partial t^2$, where $F_i(t)$, $a_i(t)$ and $r_i(t)$ are the force, acceleration and position of atom i at time t , respectively. The force on atom i is the negative gradient of the potential function which is obtained from the same EFF as used in molecular mechanics. To integrate the equations of motion, position vectors are determined using these forces and the previous positions of atoms. From this, atom velocities and temperature are evaluated. With these ingredients a trajectory, which is a history of the motion of the system over the time period of interest, can be generated. Simulation time periods are typically in the picosecond (10^{-12} s) range, so that only very fast processes such as low-energy bond rotations can be studied.

2.4. Monte Carlo simulations (MC)

This method uses the same EFFs as in MM and MD. One starts with a collection of particles and computes the system's energy, E_1 , for that initial configuration. One or more of the particles is then randomly moved to create a second configuration. The energy of this configuration, E_2 , is computed and that new configuration is deemed "acceptable" if $E_2 < E_1$ or $E_2 > E_1$ with some probability, $p = \exp[(E_2 - E_1)/kT]$. A large number of energetically feasible states are thus obtained, providing averaged energies or properties. A common application is in the assessment of the distribution of solvent molecules around solutes in solvation studies.

2.5. Molecular graphics

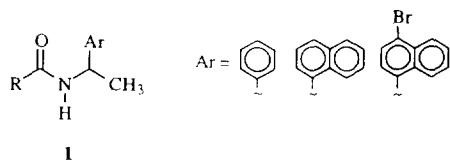
QM, MM, MD and MC calculations all generate enormous quantities of data; graphics or visualization methods render the data manage-

able and assimilable. The pictures may be graphs or simple chemical structures or they may be highlighted, three-dimensional images emphasizing structural, electronic or reactivity features of interest. With cleverness, four or five attributes of the system can be shown in a single image. Motion pictures can be created to illustrate dynamic processes. Molecular graphics temporarily uncouples the scientist from the underlying theories and equations being implemented so as to focus on the science at hand. It is an aid that helps the chemist to perceive relationships more easily and is now a standard feature of most computational programs.

Most of the molecular modeling tools are themselves models, often used in tandem to compute structures, energies and properties of molecules. Such tools along with statistics programs, relational databases and other methods for generating data are fully integrated into sophisticated molecular modeling programs. These modeling programs allow one to put together bits and pieces of seemingly unrelated, atomic-level data and create a simplified view of reality that has predictive power. This simplified representation is a molecular model and the act of creating such models is molecular modeling. Applications of molecular modeling to discern where and how chiral discrimination takes place on Type II–V CSPs are now considered.

3. Type II CSPs

The first application of atomistic molecular modeling in the area of chiral chromatography was carried out by Weinstein et al. [14]. Earlier, chiral secondary amides (**1**) were found to be suitable chiral stationary phases in gas–liquid



R = $-\text{CH}_3$, CF_3 , $n\text{-C}_3\text{H}_7$, $n\text{-C}_{11}\text{H}_{23}$, *tert.*-Bu

chromatography [15]. To begin rationalizing how this melt acted as a CSP, especially for (*R*)-*N*-lauroyl- α -(1-naphthyl)ethylamine, Gil-Av's chromatography group began working with Leiserowitz' crystallography group to carry out a series of X-ray crystallographic studies on the molecular packing modes of mono-*N*-substituted primary amides [16].

Of thirteen amides in which R is unbranched, nine form H-bonded stacks with an inter-strand spacing of 5 Å. Two other packing modes are possible: a two-fold screw axis or a glide plane, which were also observed. However, the 5 Å translational mode is the dominant motif found for these amides and it forms the basis for a model that accounts for discrimination of enantiomers.

The model is an intercalative one that assumes the bound analyte intercalates within the H-bonded array of the CSP matrix without disrupting that 5 Å, H-bonded motif. An example of the (*S*)-*N*-trifluoroacetyl- α -phenylethylamine inserted in the 5 Å stack of (*R*)-*N*-lauroyl- α -(1-naphthyl)ethylamine is shown in Fig. 1 (top) and that for the *R*-enantiomer is shown in Fig. 1 (bottom).

It was found experimentally and verified computationally that analytes with the same configuration as the CSP have longer retention times than the analytes with inverted stereocenters. Hence the example in Fig. 1 (top) corresponds to the intercalation of the first-eluted analyte. Throughout these studies, the QCFF/PI force field, developed at the Weizmann Institute, was used to determine which conformations and packing modes were most favorable. The variation in energy of the diastereomeric inclusion complexes between the guest analyte and host CSP were examined. Both intermolecular energies and intramolecular energies, given as contour plots, were evaluated, confirming the proposed model.

The collaboration between Gil-Av and Leiserowitz provides an example of atomistic molecular modeling where interaction energies between analyte and CSP are computed. To accomplish this one must have some knowledge of the shape of the CSP which, for these authors,

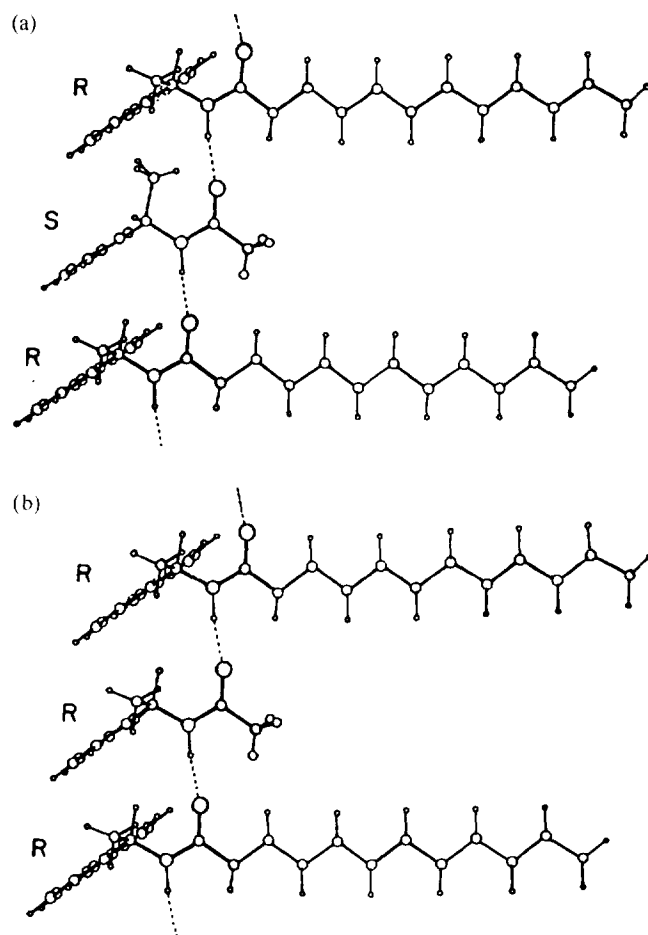


Fig. 1. Weinstein et al.'s intercalation model for chiral recognition on chiral secondary amide CSPs in gas chromatography. (a) (*S*)-*N*-Trifluoroacetyl- α -phenylethylamine inserted into the 5 Å stack of (*R*)-*N*-lauroyl- α -(1-naphthyl)ethylamine; (b) the more retained *R*-enantiomer intercalated into the same stack.

was derived from X-ray crystallography. In the case of cellulose-based phases, however, little information concerning the structure of the polymer is known and, consequently, modeling of the enantioselectivity is not feasible. Nonetheless, molecular modeling studies directed toward understanding the molecular recognition process of cellulose-based CSPs have been carried out.

For example, Isaksson et al. [17] considered analyte binding to cellulose triacetate (CTA) with statistical theories to assess the relationships between chiral recognition and symmetry of the analyte. This study was precipitated by their finding that small changes in analytes, such as

biphenyls, often led to unexpected retention times. Rather than attempt to compute the actual binding constants, they addressed how symmetry influences differential binding constants for chemically similar compounds. Their conclusion is that there is a higher probability of obtaining a good resolution for symmetrical molecules containing a proper axis of rotation (C_n axis) than for asymmetric enantiomer pairs. Further, the higher the order and number of symmetry axes, the better the separation is expected to be.

To test this theory, a set of separations were considered. Of the 216 chiral compounds consid-

ered, 36 had a least one C_n axis of symmetry and four had more than one (D_2 symmetry). A plot of the number of compounds, n , as a function of the α values, grouped in intervals of 0.2α units, was made (Fig. 2, top). Comparison of the complete set with that of a subset containing only symmetrical compounds (Fig. 2, bottom) indicated that these two distributions are different. In general, the symmetrical compounds show consistently good separations whereas the unsymmetrical compounds show poorer separations.

Another example of applying computational chemistry to understand how CTA I works was carried out by Wolf's group at Ciba-Geigy [18]. They investigated the influence of the chemical

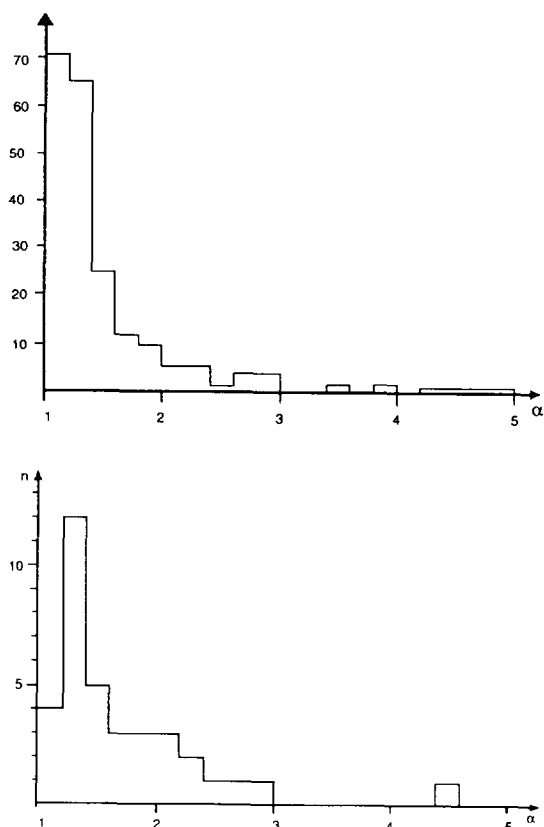
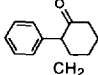
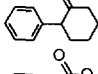
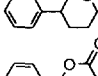
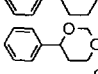
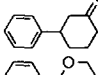
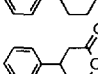
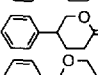
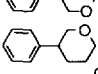
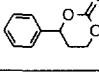
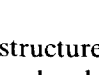
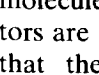
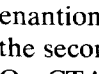


Fig. 2. Top: histogram of the number of analytes resolved on cellulose triacetate vs. their separability factors. A total of 216 compounds are represented. Bottom: the distribution of a subset (36 compounds) containing at least one C_n axis of symmetry.

Table 1
Chromatographic results: capacity factors k'_1 and k'_2 and separation factor α

Racemate	k'_1	k'_2	α
	1.2	2.6	2.2
	0.8	0.8	1.0
	1.3	4.2	3.3
	1.3	29.7	23.3
	2.4	11.1	4.6
	1.2	1.6	1.4
	1.0	3.3	3.3
	1.7	1.7	1.0
	1.5	1.5	1.0
	2.2	12.0	5.4
	0.8	0.8	1.0
	1.4	9.5	6.8

structure for a series of related racemates. The molecules, capacity factors and separability factors are presented in Table 1. It should be noted that the capacity factors for the first-eluted enantiomer are about the same whereas those of the second-eluted enantiomer span a large range. On CTA I a large k'_2 value almost always leads to a high α . Hence these authors decided to use k'_2 as the important experimental parameter to be correlated with their computed molecular descriptors. They attempted to find quantitative molecular descriptors for these twelve analytes and to correlate those descriptors with their chromatographic data. These molecular properties, it must be emphasized, are independent of the configuration of the analyte so no stereochemical arguments can be made.

Two criteria seemed important in the chiral separations. First, as had been noted by many

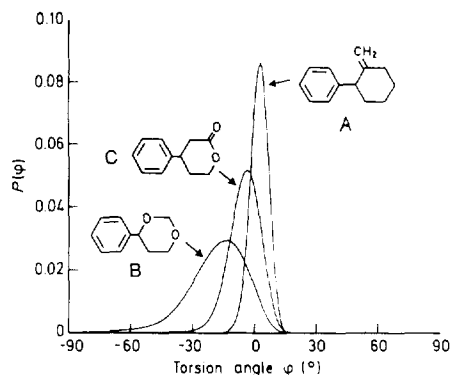


Fig. 3. Boltzmann distribution of the conformational states of the three classes of compounds displaying very restricted, intermediate and high conformational freedom.

authors, the shape of the analyte seems important, and second, all compounds containing an oxygen adjacent to the stereogenic center have large k'_2 values indicating that negative charge adjacent to that center enhances resolution. These two effects are, experimentally, inexorably linked; placing an sp^3 oxygen α to the stereogenic center provides the requisite electron density but, by replacing the *exo*-methylene or carbonyl groups with this oxygen, it makes the analyte more flexible owing to easy rotation around the phenyl group.

Conformational studies (shape descriptor) were carried out with molecular mechanics and atomic charges used to create molecular electrostatic potential maps (electronic descriptor) were

done with quantum mechanics. The authors examined the rigidity of the analyte by Boltzmann weighting the conformational energies for all analytes. They found that the twelve analytes could be partitioned into three categories, depicted in Fig. 3. One grouping, represented by A in Fig. 3, has a very narrow probability distribution and may be considered "rigid". In Fig. 3 a 0° dihedral angle means that the phenyl ring is orthogonal to the saturated ring. Hence these rigid molecules will never become planar (it is presumed that flat molecules generally fit better into the chiral cavities or crevices of CTA I than do non-planar molecules). The second category, represented by molecule B in Fig. 3, has a broad distribution of conformational states and can adopt near-planar shapes. The third category is between the "stiff" and the "flexible" analytes. It turns out that the flatness of the analyte alone is not the only factor responsible for good complexation with CTA. To probe the electronics of these analytes, the authors computed molecular electrostatic maps as in Fig. 4 and extracted from them a normalized electrostatic interaction energy.

The two molecular descriptors thus used were $[\Omega]$, a measure of flatness, and E_{00} , a measure of negative charge distribution around the stereogenic carbon. Using these two simple descriptors, a regression model was developed:

$$\ln k'_2^{(i)} = AE_{00}^{(i)} + B[\Omega]^{(i)} + C \quad (i = 1-12) \quad (1)$$

where $A = -0.122$, $B = 0.0211$ and $C = 0.497$.

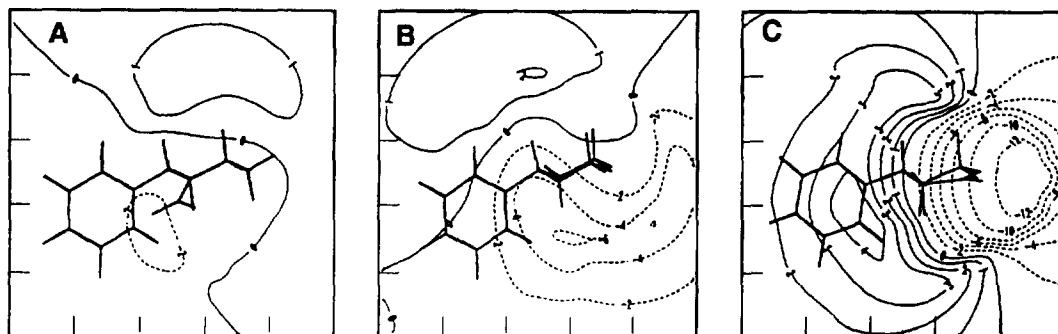


Fig. 4. Molecular electrostatic contour maps for molecules A, B and C in Fig. 3. Contour lines are in units of kcal mol^{-1} , full lines represent positive regions and broken lines represent negative regions.

Using this model, the authors predicted k'_2 values for comparison with experiment and found a good correlation (correlation coefficient = 0.96).

Other attempts to quantify the effect of structural parameters on the separation of enantiomers of CTA I have been reported. Most notable is the work by Roussel and his group in France, who use full factorial design to quantify the effect of structural parameters (factors) on either the separations or capacity factors (responses) of atropisomeric isomers on CTA I [19]. In this way one can quantitate the variables responsible for retention and separation.

The three structural modifications are shown in Fig. 5. Since there are three changes being made there must be $2^3 = 8$ molecules to explore fully (for three changes at two levels) the recognition process. X_1 can be oxygen (level -1) or sulfur (level +1); X_2 can be hydrogen (level -1) or methyl (level +1); X_3 can be hydrogen (level -1) or methyl (level +1). These eight test probes were synthesized and resolved on CTA I. If one assumes linearization of the influence of substituent patterns for each enantiomer, by difference, one can assess the enantioselectivity. This linearization is expressed by the equation

$$Y = c_0 + c_1X_1 + c_2X_2 + c_3X_3 + c_{12}X_1X_2 + c_{13}X_1X_3 + c_{23}X_2X_3 + c_{123}X_1X_2X_3 \quad (2)$$

where Y is the response, X_1 , X_2 , X_3 are the primary effects and X_1X_2 , X_1X_3 , X_2X_3 , $X_1X_2X_3$ are the bilinear and trilinear cross-terms. The c_s are the coefficients for each term determined from solving the eight equations, from eight experiments, by replacing the X_i with +1 or -1 according to the experiment. A positive coefficient

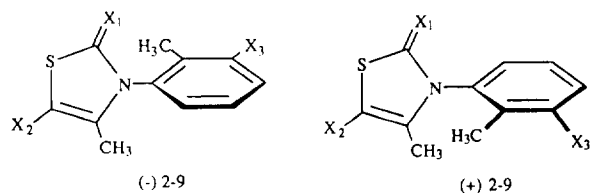


Fig. 5. Structures of the N-arylthiazoline-2-thiones and N-arylthiazolin-2-ones used by Roussel et al. X_1 = oxygen or sulphur; X_2 = hydrogen or methyl; X_3 = hydrogen or methyl.

Table 2
Compounds, design levels and responses

Compound	Design level			Response		
	X_1	X_2	X_3	$k'(+) $	$k'(-) $	k'_2/k'_1
2	-	-	-	2.05	1.66	1.24
3	+	-	-	1.52	2.30	1.51
4	-	+	-	0.66	0.55	1.21
5	+	+	-	0.87	0.78	1.12
6	-	-	+	0.81	1.92	2.36
7	+	-	+	0.96	3.09	3.20
8	-	+	+	0.35	0.35	1.00
9	+	+	+	0.64	0.61	1.04

means that on going from the low level to the high level of that factor, the response is increased. A negative coefficient, in turn, means the response is decreased. Table 2 lists the molecules studied, their design levels and chromatographic results.

Eq. 3 is derived for the (+)-enantiomer and Eq. 4 for the (-)-enantiomer:

$$k'(+) = 0.98 + 0.015X_1 - 0.35X_2 - 0.29X_3 + 0.11X_1X_2 + 0.09X_1X_3 + 0.15X_2X_3 - 0.075X_1X_2X_3 \quad (3)$$

$$k'(-) = 1.40 + 0.29X_1 - 0.83X_2 + 0.08X_3 - 0.16X_1X_2 + 0.07X_1X_3 - 0.17X_2X_3 - 0.06X_1X_2X_3 \quad (4)$$

For the dextrorotatory isomer, the primary interactions most dominant are X_2 and X_3 . The sign and the magnitude of these coefficients indicate that on going from a low level (H) to a high level (Me) at either C-5 on the thiazoline or C-3' on the aryl ring, steric effects between analyte and CSP decrease the capacity factor. The relatively small coefficient for X_1 means replacing the ketone with a thione has a minor influence on the dextrorotatory enantiomer retention.

For the levorotatory isomer, the most important primary effects are X_1 and X_2 . Hence for this enantiomer replacement of the carbonyl with a thiocarbonyl has a substantive impact on re-

tention whereas replacing the H with Me on the aryl C-3' has almost no effect on retention. The dominant primary effect is still due to X_2 .

From this kind of analysis (a full discussion of the significance of the cross-terms is given in the original paper), Roussel et al. were able to address which parts of the analytes were most sensitive for both enantiomers binding to the CTA I CSP. This type of computational approach is complementary to the work described by Isaksson [17] and by Wolf et al. [18], and it has great promise for unraveling how the complex intermolecular forces responsible for chiral separation work.

An extension of this work was done by Roussel and Popescu [20], who developed a lipophilicity parameter, $\log k'_w$, by extrapolating plots of $\log k'$ in methanol–water solvents (on an alkyl-bonded stationary phase) to 100% water. Separation of atropisomers **2–9** on CTA I and *tris*(*p*-methylbenzoyl)cellulose beads (CTPB) resulted in five measured responses: $\log k'_w$, $\ln k'(+)$ -CTA, $\ln k'(-)$ -CTA, $\ln k'(+)$ -CTPB and $\ln k'(-)$ -CTPB. The derived coefficients are as follows:

$$\begin{aligned} \log k'_w = & 3.14 + 0.001X_1 + 0.256X_2 + 0.226X_3 \\ & - 0.01X_1X_2 - 0.01X_1X_3 - 0.006X_2X_3 \\ & + 0.01X_1X_2X_3 \end{aligned} \quad (5)$$

$$\begin{aligned} \ln k'(+)\text{-CTA} = & -0.14 + 0.09X_1 - 0.36X_2 \\ & - 0.28X_3 + 0.12X_1X_2 \\ & + 0.09X_1 + 0.09X_1X_3 \\ & + 0.05X_2X_3 - 0.01X_1X_2X_3 \end{aligned} \quad (6)$$

$$\begin{aligned} \ln k'(-)\text{-CTA} = & 0.09 + 0.21X_1 - 0.68X_2 \\ & - 0.03X_3 + 0.01X_1X_2 \\ & + 0.04X_1X_3 - 0.14X_2X_3 \\ & + 0.007X_1X_2X_3 \end{aligned} \quad (7)$$

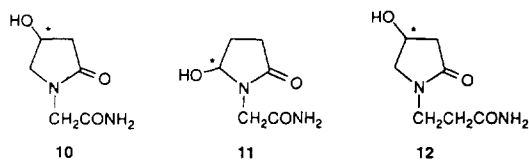
$$\begin{aligned} \ln k'(+)\text{-CTPB} = & 0.67 + 0.60X_1 - 0.13X_2 \\ & - 0.12X_3 + 0.05X_1X_2 \\ & + 0.05X_1X_3 + 0.01X_2X_3 \\ & + 0.006X_1X_2X_3 \end{aligned} \quad (8)$$

$$\begin{aligned} \ln k'(-)\text{-CTPB} = & 0.62 + 0.74X_1 + 0.11X_2 \\ & - 0.91X_3 + 0.09X_1X_2 \\ & - 0.18X_1X_3 - 0.01X_2X_3 \\ & - 0.04X_1X_2X_3 \end{aligned} \quad (9)$$

Using the same kind of analysis as above, the authors were able to explain the relationship between chiral retention of the enantiomers and their lipophilic interactions with the CSPs. Quantification of the influence of structural parameters X_1 , X_2 and X_3 was possible. The relationship between lipophilicity and chiral chromatographic behavior was explained for compounds **2–9** and an extension to other alkyl-substituted atropisomers was made along with rationalization for unexpected results. A related study on the resolution of **2–9** on various *p*-methylbenzoylcellulose beads has also been published [21].

Molecular modeling studies of enantioselectivity by the cellulose triphenylcarbamate CSP has been reported by Camilleri et al. [22]. They carried out separations of oxiracetam (**10**) and two related molecules (**11** and **12**) on a Chiracel OC column. For modeling purposes they generated a trisaccharide of β -1,4-linked D-glucoses, end-capped with methyls. Energy minimization with quantum mechanics gave a linear structure with intramolecular H-bonds. The hydroxyls were replaced with phenylcarbamate residues and the resulting trisaccharide was energy minimized again. The phenyl carbamate groups induce a helical twist to the polymer owing to steric repulsions of the phenyls, but the helicity of the CSP was dismissed as being responsible for chiral recognition.

After manual docking of the analyte with CSP, energy minimization with molecular mechanics was performed. It was found that only for the *R*-isomer of **10** could a viable three-point as-



sociation exist, which explains why the *R*-isomer is retained longer than the *S*-isomer. With the aid of molecular modeling, the authors were able to identify possible interactions leading to stereoselection.

Most of the computational studies of type II CSPs have not considered the CSP directly. Instead, regression models are constructed to explain how a set of probe molecules interact with the CSP. The example above by Camilleri et al. sets forth an explicit treatment of the CSP. Other examples where the CSP is explicitly modeled have been published.

One example is by Alkorta et al. [23]. Here the molecular modeling involved correlating the molecular mechanics binding energies of substituted benzenes, phenols and naphthalene with retention orders on CTA I. Eventually a linear relationship between $\log k'$ and the interaction energies was obtained. This study does not explain chiral interactions but it does introduce a picture of what the CSP looks like. Another example of modeling the structure of these type II CSPs is presented by Francotte and Wolf [24]. They prepared and evaluated benzoylcellulose beads in a pure polymeric form as a sorbent for the chromatographic resolution of racemic compounds such as benzylic alcohols and acetates of aliphatic alcohols and diols. Their results implicated multiple interaction sites to be involved in the complexation. A rationalization of the interaction mechanism required a more systematic investigation of the factors influencing separations and, to address the structural features of the cellulose tribenzoate, they carried out molecular modeling with molecular mechanics. The key question being addressed is the extent to which the polysaccharide backbone is exposed to small molecules when sterically encumbered benzoates are attached.

Representative decameric chain segments were generated by excising the third unit of an energy-minimized hexamer as their monomer. This monomer was polymerized, *in computero*, using the glycosidic bridge angles between the two middle segments to create the polymer backbone. In this way the computational artifact of having terminal end-groups is eliminated. Color-coded molecular graphics displays of the

decameric strands in two low-energy conformations revealed that the sugar residues are able to interact, at least partially, with small molecules so that the chiral discrimination does not come solely from the benzoyl groups.

Another study is by Lipkowitz' group [25], who repeated an earlier study on the crystal packing of cellulose triacetate reported by Wolf and Scheraga [25]. Similar results were found using different force fields (MM3, AMBER) than that used by Wolf and Scheraga (ECEPP-2). A display of the disaccharide making up the unit cell, a sheet of these polymers and a microcrystallite of CTA I are presented in Fig. 6. Lipkowitz' group is currently examining averaged structural features of the monomers, inter-strand geometries and dynamic properties of these microcrystallites from molecular dynamics simulations in an attempt to understand where analytes bind. Eventually, their goal is to simulate the binding of analytes like those in Table 1 to understand enantiodifferentiation based on atomistic modeling.

The helical conformations and conformational stability of isotactic poly(triphenylmethyl methacrylate) have been investigated by Vacatello's group [26] in Italy using an empirical force field. For their preliminary analysis they considered a dimer and omitted several of the phenyl rings to simplify the calculations. The authors acknowledged that not all the conformations for the dimer will be allowed in longer chains and, accordingly, they generated a hexameric unit. It was found that only one backbone conformation is allowed for helical segments with the two-bond repeat unit and that the polymer has approximately 3.6 monomers per turn with a 2.0 Å pitch per monomer unit. Their conclusion is that the polymer is composed of $\dots |G^+T|G^+T| \dots$ and $\dots |TG^-|TG^-| \dots$ with $G^+ \approx +75^\circ$, $G^- \approx -75^\circ$ and $T \approx \pm 160^\circ$. This motif firmly locks in the side groups and the interconversion between P and M helices is inhibited by a large energy barrier. No analyte binding studies have been reported by this or any other group, however.

Finally, we mention here the work by Ning [27] on salting effects in reversed mobile phases for the chiral separation of both *cis*- and *trans*-benzonaphthazepine enantiomers on cellulose

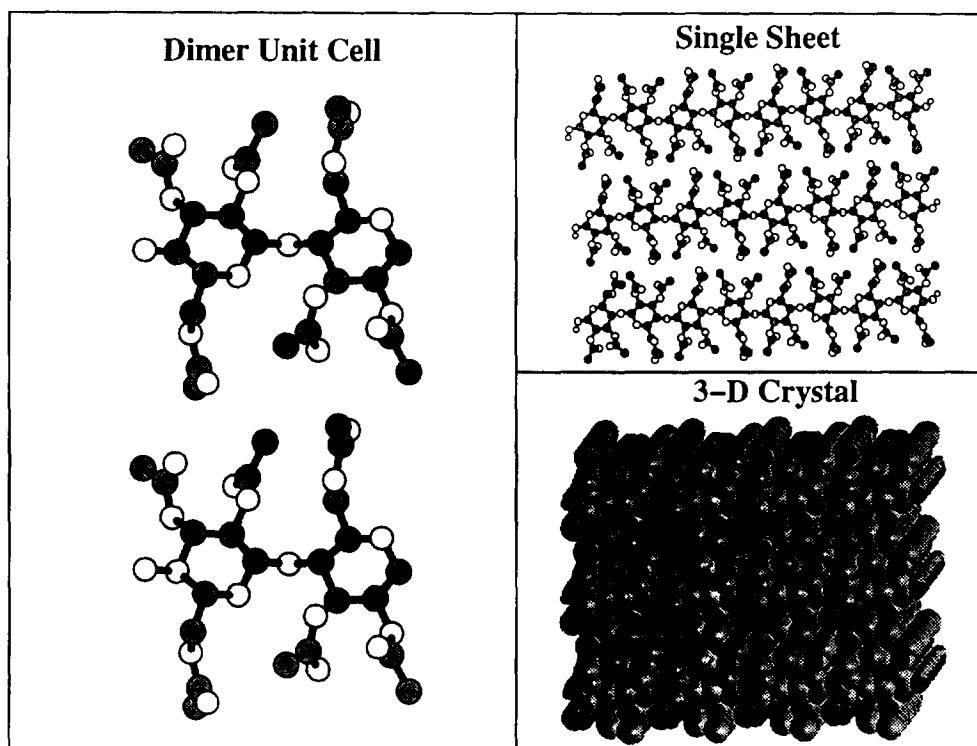


Fig. 6. The unit cell of CTA I consists of two disaccharides. Three strands of crystallite are shown on the top right and a space-filling model of a microcrystallite, with spacings consonant with X-ray data, is shown on the bottom right. Hydrogen atoms are omitted for clarity.

tris(3,5-dimethylphenylcarbamate) CSP. The salting-in effect of NaClO_4 makes the analytes more soluble in the mobile phase so that the CSP can selectively retain the four stereoisomers. The salting-out effect of NaCl induces hydrophobic self-association and, accordingly, the author proposed that the NaCl works differently than a conventional ion-pair reagent in non-chiral reversed-phased chromatography.

Experimentally, the retention order is (-)-*trans*, (-)-*cis*, (+)-*trans*, (+)-*cis*. This order is unusual and was rationalized by atomistic molecular modeling. Using molecular mechanics, the lowest energy conformers for both *cis* and *trans* analytes were located. Ning then discovered that the *cis* isomer can be superimposed almost perfectly on top of the *trans* diastereomer. In contrast, two enantiomers do not possess such perfect matching. Hence, when a *cis* diastereomer encounters a *trans* diastereomer they are forced, by hydrophobic effects, to form a dimer

that moves into and out of the mobile phase until they become trapped in a suitable cavity of the CSP. There they are further discriminated. By comparison, the enantiomers do not match well when forced together and are proposed to be moving about individually, randomly associating with the CSP and being well resolved. This proposal rationalizes why the corresponding diastereomer rather than the enantiomer follows in the separation. Finally, because the *trans* isomer has a smaller pucker angle by 6° than does the *cis* isomer, it has less steric bulk and should elute less quickly than the *cis* isomer. This is consonant with experiment.

Most of the molecular modeling studies of type II CSPs, as we see from above, do not directly involve interaction of the analyte with the CSP to discern where and how chiral recognition takes place. This is in contrast to modeling of brush-type CSPs previously reviewed [12] and type III CSPs discussed below. The reason for

this is, apparently, the lack of structural information about these CSPs. It is anticipated, however, that one will soon find direct analyte–CSP computations to discern where and how chiral separations take place.

4. Type III CSPs

Type III CSPs work by forming inclusion complexes and two main categories of host molecules have been studied computationally. These are cyclodextrins (CDs) and their derivatives and crown ethers. In a series of papers, Armstrong and co-workers used molecular graphics representations of how β -CD separates diastereomers [28] and enantiomers [29,30]. These graphic images were presented in color to highlight similarities and differences of analyte binding, but these studies did not involve complete energy minimizations. Using rigid cyclodextrin, the authors allowed only the important torsion angles and the location of the analyte in the macrocycle to change. The modeling highlighted the importance of the 2- and 3-hydroxyl groups for the resolution of enantiomers and allowed the authors to design rationally derivatives of CDs to optimize a particular separation.

This led Boehm et al. [31] to formulate a statistical thermodynamic theory of chiral solute retention and separation on models of chemically bonded CSPs. For an infinitely dilute solution, the capacity factor for a distribution of solute molecules between two phases is $k = \exp(-\beta \Delta A)$, where $\beta \Delta A$ represents the Helmholtz free energy accompanying the transfer of solute from the mobile phase to the stationary phase. When the mobile phase is non-chiral and all the interactions of solvent molecules with individual enantiomers are identical, the equation

$$\alpha = k_D/k_L = \frac{\sum_i \exp(-E_{i,D}/kT)}{\sum_j \exp(-E_{j,L}/kT)} \quad (10)$$

holds where $E_{i,D}$ and $E_{j,L}$ are the interaction energies of D- and L-enantiomers in their i th and

j th modes of retention on the CSP. In Eq. 10 one must specify the complete set of $E_{i,D}$ and $E_{j,L}$ available to the system. This requires introducing a model for both solute and CSP. Models for CDs were provided which consist of truncated conical cavities with three or more binding domains on the periphery of one rim and a fourth site attached to silica.

Chiral tetrahedral analytes with four groups a, b, c and d are presumed to interact with three sites 1, 2 and 3 on the CSP by simultaneous three-site, two-site and one-site interactions. There are twelve three-site CSP–analyte interactions, 36 two-site interactions and twelve one-site interactions, giving 60 possible, distinctly unique types of $E_{i,D}$ and $E_{j,L}$ interactions, all of which can contribute to the total interaction energies for D- and L-analytes. Of these possible combinations some are different for the D-enantiomer when compared with the L-enantiomer and these are the interaction modes that can lead to separation. For a tetrahedral analyte with groups abcd embedded in the interior of a CD with domains 1234, there are twelve different four-site, twelve different three-site, 36 different two-site and twelve different one-site interaction modes possible. Only the four- and three-site modes are enantiodiscriminating.

An estimation of the separability factor in Eq. 10 requires evaluation of the ratio of the sums of the two Boltzmann weighted terms, summed over all the interaction modes possible. When one mode of interaction predominates over all others, the summations in Eq. 10 can be approximated by those dominant terms alone. If there is a single dominant mode of retention, denoted by Boehm as $E_{i^*,D}$ and $E_{j^*,L}$, Eq. 10 reduces to

$$\alpha = \exp[-\beta(E_{i^*,D} - E_{j^*,L})] \quad (11)$$

where $\beta = 1/kT$. When the retention for each enantiomer is dominated by a single chirally discriminating mode of retention, Eq. 11 is approximated by $\alpha = \exp(\beta \Delta E)$. Thus $\ln \alpha$ is a linear function of both adsorption energy and the reciprocal of temperature. The slope of $\ln \alpha$ vs. $1/T$ will provide ΔE of D- vs. L-analyte in their dominant retention mode and variation from linearity indicates mixed modes.

Rather than dwell on hypothetical interactions, Berthod et al. [32] devised a scheme for attributing individual substituent contributions to chiral recognition by (*R*)-(-)-1-(1-naphthylethyl)carbamoylated β -CD CSP (*R*-NEC- β -CD) and the corresponding (*S*)-(+)-phase (*S*-NEC- β -CD). The objective was to be able to predict whether or not an analyte with four different substituents connected to the stereogenic center would be resolvable on these CSPs. The separability factor, α , is due to the chiral interactions for enantiomer 1 and enantiomer 2 by $\alpha = \exp \Sigma [(\Delta G_{c1} - \Delta G_{c2})/RT]$. The differential free energy due to the chiral interaction of the two enantiomers, $\Delta\Delta G_c$, was divided into four terms, each representing one of the four groups as in the equation

$$\begin{aligned} \Delta\Delta G_c = & (\Delta G_{c11} - \Delta G_{c12}) + (\Delta G_{c21} - \Delta G_{c22}) \\ & + (\Delta G_{c31} - \Delta G_{c32}) + (\Delta G_{c41} - \Delta G_{c42}) \end{aligned} \quad (12)$$

It is assumed that the chiral interaction contributions are independent of one another and that the interactions are additive and, accordingly, predictive.

A total of 126 compounds were analyzed on these two CSPs. However, only 81 unique groups exist in their data set owing to redundancy. The hydrogen substituent was arbitrarily set equal to 0 cal/mol for a chiral free energy contribution and the authors noted that changing this arbitrary value would influence the sign of some substituents contributions. The authors generated one equation (Eq. 12) for each compound studied, and, setting $\Delta G_H = 0$ cal/mol, solved the equations while the error function $E = \Sigma |\alpha_{\text{calc}} - \alpha_{\text{obs}}|$ was minimized. If the substituent has a positive value it means an enhanced chiral recognition by the NEC- β -CD CSP exists compared with H, and a negative energy value means the opposite.

Generally, the chiral recognition increased when sp^2 carbons are attached to the stereogenic center and decreased when sp^3 carbons are attached to the stereogenic carbon. The effects of π - π stacking, hydrogen bonding and dipole stacking were also assessed. Although this meth-

od does not allow one to predict an elution order, the substituent constants (for those CSPs) can be used to make an estimate of the enantioselectivity of an unknown by adding the energy contributions of the four substituents connected to the stereogenic carbon of that unknown compound.

A slightly different approach was taken by Roussel and Favrou [33] toward understanding chiral separations by cyclodextrins and quantifying the effect of substituents. Using compounds (-)-2-9 and (+)-2-9, the authors carried out chiral separations using β - and γ -cyclodextrins as a chiral mobile phase additives. The full factorial design methodology was applied to k'_0 (retention without cyclodextrin), $k'_0(+)$, $k'_0(-)$ and α for two different achiral stationary phases. In the presence of γ -CD on a non-end-capped phase, the following equations were derived:

$$\begin{aligned} k'_0 = & 86.43 - 2.77X_1 + 33.39X_2 + 31.70X_3 \\ & - 6.19X_1X_2 - 2.74X_1X_3 + 12.73X_2X_3 \\ & - 3.43X_1X_2X_3 \end{aligned} \quad (13)$$

$$\begin{aligned} k'_0(+) = & 20.92 - 6.15X_1 + 7.31X_2 + 8.17X_3 \\ & - 2.65X_1X_2 - 2.81X_1X_3 + 3.00X_2X_3 \\ & - 1.27X_1X_2X_3 \end{aligned} \quad (14)$$

$$\begin{aligned} k'_0(-) = & 20.65 - 6.25X_1 + 7.14X_2 + 8.44X_3 \\ & - 2.65X_1X_2 - 2.71X_1X_3 + 3.17X_2X_3 \\ & - 1.27X_1X_2X_3 \end{aligned} \quad (15)$$

$$\begin{aligned} \alpha = & 1.024 + 0.016X_1 + 0.008X_2 - 0.024X_3 \\ & + 0.008X_1X_2 - 0.016X_1X_3 - 0.008X_2X_3 \\ & - 0.008X_1X_2X_3 \end{aligned} \quad (16)$$

From Eq. 13, one finds that without γ -CD, two structural features, X_2 and X_3 , have a predominant influence on retention. A change in electrostatics by converting the carbonyl to thiocarbonyl does not have much influence on the capacity factor. In contrast, when γ -CD is present, Eqs. 14 and 15 show X_1 , X_2 and X_3 to affect retention similarly for each atropisomer, and these influences are weak. In the presence of the chiral modifier γ -CD, then, the change from carbonyl to thiocarbonyl becomes important with the latter being more retained. Finally, from Eq. 16,

X_1 and X_3 are most important. Similar analyses for stability constants were addressed and an attempt to assess factors responsible for β -CD as a mobile phase additive were made. Optimization of the separations by varying the EtOH percentage and the nature and pH of the buffer were attempted, but chiral discrimination was mainly influenced by the CD cavity size and strength of the inclusion complex.

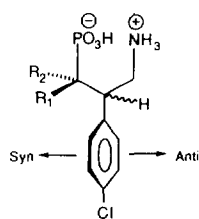
The chromatographic behavior of phaclofen (**13**) and its difluoro derivative (**14**), along with the diastereomeric monofluoro species **15** and **16** on acetylated β -CD has been studied. In methanol/aqueous triethylamine–acetic acid, **13** is not resolved but **14** is with $\alpha = 1.11$. Further, **16** is resolved but not **15**. A theoretical model for this behavior, in terms of the asymmetry in the π -facial molecular electrostatic potentials on the phenyl ring, was presented [34]. Using semi-empirical molecular orbital theory the electrostatic potentials on the *syn* and *anti* faces of the aryl ring were determined. Those analytes with larger electrostatic differences between *syn* and *anti* faces appear to correlate with separations, but precisely how this electrostatic asymmetry works was not explained.

Most of the aforementioned studies represent quantitative structure–retention relationship studies where a series of analytes are used as probes of enantiodiscrimination. There are, however, a number of atomistic molecular modeling studies where the interactions of chiral guests (analytes) with chiral hosts (CSPs) are explicitly determined. Before reviewing these papers, we point out that most of the published computational studies of cyclodextrins (CDs) involve examination of their structures with MM or MD techniques or, using quantum mechanics, to rationalize their proclivity to bind non-chiral

guests in a particular orientation. Also, an analysis of the shapes of cyclodextrins exists [35] and a comparison of α -, β - and γ -CDs in the solid state was made for native and derivatized species. Features of the CD monomer units, including orientations of 1° OH groups and pyran ring pucker, were presented. Macromolecular features described for these host molecules include planarity of the macrocycle, tilt of the pyran rings and deviations from six-, seven- and eightfold symmetry for α -, β - and γ -CDs, respectively. The mean values and standard deviations for these shape descriptors were given, making this an especially valuable reference.

Atomistic molecular modeling studies where guest and host are considered as transient diastereomeric complexes have been published. Both liquid and gas chromatographic studies have been modeled. For example, from work by Armstrong et al. [36] it was known that (*R*)-tryptophan binds more tightly to an α -CD column than does (*S*)-tryptophan with $\alpha = 1.20$. To understand this enantioselection, Lipkowitz et al. [37] used molecular dynamics simulations to answer the following questions: (a) what are the intermolecular forces responsible for analyte binding to the CSP?; (b) where on or in the host does the analyte bind?; (c) what are the differential interactions giving rise to chiral discrimination?; (d) what differences do (*R*)- and (*S*)-tryptophan experience in the CD cavity?; and (e) are existing chiral recognition mechanisms valid?

Using the CHARMM force field for molecular dynamics, the authors' simulations reproduced both the correct retention order and separability factor from chromatography in addition to the intermolecular and intramolecular NOE observations from their NMR experiments. Total averaged energies were partitioned into their component terms. The more tightly bound *R*-enantiomer was favored computationally because its complex had less torsional strain and because the non-bonded interactions are more favorable. Both analytes had similar electrostatic components, however. These component energies were also partitioned into internal energies (intramolecular energies) and external energies (inter-



- | | |
|-----------|--------------------|
| 13 | $R_1 = R_2 = H$ |
| 14 | $R_1 = R_2 = F$ |
| 15 | $R_1 = H, R_2 = F$ |
| 16 | $R_1 = F, R_2 = H$ |

molecular energies). Both internal and external energies favor the *R*-analyte.

Because intermolecular H-bonding was considered to be important, the authors evaluated the number and kinds of intermolecular H-bonds between guest and host. They found that not only does the more retained *R*-enantiomer form more H-bonds than does the *S*-enantiomer, but also that these H-bonds are usually simultaneous, multiple-contact H-bonds between guest and host. An illustration summarizing their results is depicted in Fig. 7.

Three key features emerge from this illustration. First, both complexes are highly localized on the interior of the CD with the *R*-enantiomer binding to one side of the macrocycle and the *S*-enantiomer to the other. Second, the *R*-enantiomer forms almost twice as many intermolecular H-bonds (2662) than does the *S*-enantiomer (1307) and, as pointed out above, they are of the multiple-contact type. Third, the hydrogen bonding occurs primarily from tryptophan's carboxylate and indole N–H but not the ammonium group. Based on this, the authors confirmed an earlier recognition model proposed

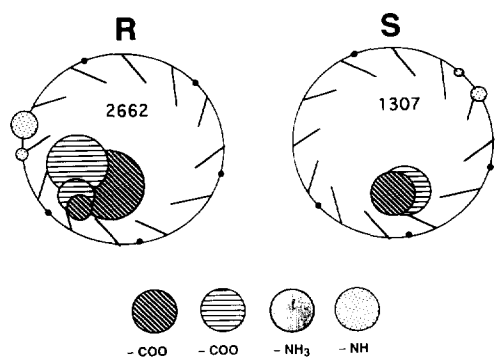
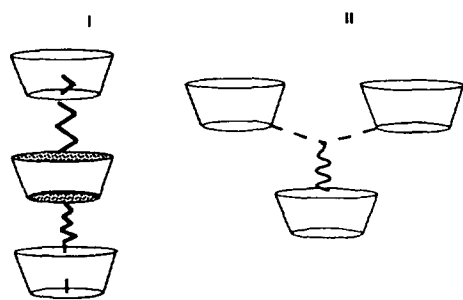


Fig. 7. Graphical representation of the intermolecular hydrogen bonds of (*R*)- and (*S*)-tryptophan with α -cyclodextrin. The large circle represents the macrocyclic host. The small black dots on that circle are the acetal linker oxygens, and the lines attached to the circle represent the unidirectional C-2 and C-3 hydroxyl groups. The cross-hatching indicates the atoms or groups of atoms on the tryptophan that are forming the intermolecular hydrogen bonds. The size of the cross-hatched circle corresponds to the number of hydrogen bonds formed during the simulation. The centers of the cross-hatched circles are placed at the mean positions of the hydrogen bond contacts.

by Armstrong but pointed out that a high degree of localization is tantamount to a tight fit in the CD cavity as promulgated by Armstrong.

Another paper by this group was published [38]. It does not involve chromatography directly but it does have a direct impact on understanding chiral discrimination in cyclodextrins. In that study the authors searched the crystallographic literature for cyclodextrins with enantiomerically pure *R* and *S* guests. Using molecular mechanics they first computed the binding enthalpy, ΔH , for each guest by comparing the molecular mechanics energy of the guest–host complex with that of the guest and host infinitely separate, i.e., $\Delta H = H_{\text{bound}} - H_{\text{free}}$. Doing this for the (*R*)-CD complex and for the (*S*)-CD complex allowed them to compute $\Delta\Delta H = \Delta H_R - \Delta H_S$, which is the enantiodiscriminating enthalpy. It was found that the dominant force responsible for guest–host complexation is the short-range London force. The enantiodiscriminating forces tended to be very small and are generally, but not always, dominated by the long-range Coulomb force. It was also found that enhanced enantioselectivity occurs in the derivatized CDs compared with the CDs in their native state. It is not clear why this occurs but the following observation was made. The native CDs, when they form guest–host complexes, form stacked or skewed columns of CDs with guests embedded along these stacks. The guest is found on the interior of the host molecule or slightly above/below the interior. This is represented by structure I. In contrast, the derivatized CDs tend to have a guest embedded in the interior (or slightly above the interior) of one host molecule but protruding into the interstitial region between CDs of the next layer. This is depicted in structure II.

In the derivatized examples, then, there is a large amount of intermolecular contact with the *exterior* of the CDs, whereas there is only *interior* contact with the native CDs. The conclusion derived by the authors is that enhanced chiral discrimination can take place on the exterior of the CD compared with the interior. This statement is noteworthy, but remains highly speculative given the limited number of systems studied.



The concept of chiral recognition on the exterior of the CD is especially relevant to gas chromatography. One of the predominant forces for guest–host complexation in aqueous phase liquid chromatography is the hydrophobic force. This is absent in the gas phase and consequently it is not clear what forces induce an analyte to bind as an inclusion complex in CD stationary phases used in gas chromatography. Indeed, from an extrathermodynamic analysis of analyte binding to derivatized cyclodextrins in the gas phase, Berthod et al. [39] suggest that both exterior and interior binding modes are possible. Exterior binding and/or partial inclusion complexation seem consistent with molecular mechanics and dynamics calculations showing these otherwise toroidal macrocycles to collapse upon themselves in the gas phase [40]. However, all publications to date assume that binding takes place in the interior.

The pioneering paper on using molecular dynamics simulations to understand chiral gas chromatographic results was published by König's group [41]. Experimentally they found the *S*-enantiomer of methyl-2-chloropropionate to be more retained on Lipodex D [heptakis-(3-*O*-acetyl-2,6-di-*O*-pentyl)- β -CD] coated on a capillary column at 333 K. A large separability factor, $\alpha = 2.02$, corresponding to $\Delta\Delta G = 2 \text{ kJ mol}^{-1}$, was observed and an attempt to discern the structural features of the transient complexes was made.

Using a known β -CD neutron diffraction structure, the authors homogeneously fixed the C-2 and C-3 substituents upward and the C-6

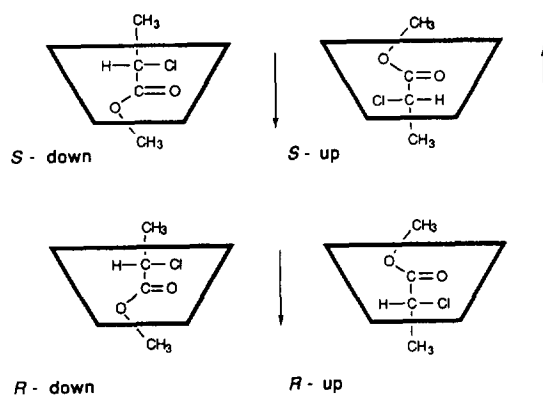


Fig. 8. Initial orientations selected for (*R*)- and (*S*)-2-chloromethylpropionate in Lipodex D for molecular dynamics simulations. The wider rim corresponds to the C-2 and C-3 groups and the narrow rim corresponds to C-6 substituents.

pentyl groups downward. The analytes were placed into the interior of the resulting cavity in “up” or “down” orientations as depicted in Fig. 8. Upon providing kinetic energy to the system, the authors found the “down” orientation led to immediate expulsion of guest from the host cavity. The *R*-“up” orientation migrated outside of the cavity but remained near the hydrophobic side-chains and the *S*-“up” complex was found to be most stable. These results are consistent with the GC results and agree with nuclear Overhauser effect results from their NMR studies showing the methyl ester near the C-3 groups of the CSP. The authors indicated that a 5-ps simulation is too short to provide unequivocal results and indicated that longer trajectories would be needed.

In a follow-up study the authors carried out longer simulations [42]. The computed complexation energy difference, favoring the *S*-enantiomer, is $5.75 \text{ kcal mol}^{-1}$ at 300 K (experimental $\Delta\Delta G = 0.65 \text{ kcal mol}^{-1}$) and at 333 K it is favored by $1.12 \text{ kcal mol}^{-1}$ (experimental $\Delta\Delta G = 0.47 \text{ kcal mol}^{-1}$) ($1 \text{ cal} = 4.184 \text{ J}$). In this paper the authors considered the shape of the host, showing that “self-inclusion” takes place when no host is present, and the shape of the analyte in both the free and complexed states. From their simulations they were also able to

deduce the time-averaged orientation in the CSP host cavity, evaluate the geometry of the guest–host complex and describe intermolecular distances between the enantiomeric analytes and chiral cavity.

Koen de Vries et al. [43] likewise found that a combined molecular mechanics and molecular dynamics approach is a valuable tool for rationalizing qualitative gas chromatographic trends. Experimentally they evaluated the thermodynamic parameters (ΔG , $\Delta\Delta G$, ΔH , $\Delta\Delta H$, etc.) for guest–host complexation of six analytes on a variety of derivatized CD columns. Their interpretation of the results was that one enantiomer fits the CD cavity better than the other, resulting in a larger interaction energy and greater loss of mobility. To help understand this, they studied the binding of one analyte (styrene oxide) to several cyclodextrins including octakis-(3-O-trifluoroacetyl-2,6-di-O-methyl)- γ -CD, octakis-(2,3,6-tri-O-methyl)- γ -CD, octakis-(3-O-acetyl-2,6-di-O-methyl)- γ -CD and heptakis-(3-O-trifluoroacetyl-2,6-di-O-methyl)- β -CD. No interaction energies were reported. Rather, attention was paid to how molecules generally tend to align in the cavity of these CSP analogs.

Kobor et al. [44] also used molecular modeling to examine how polar and non-polar analytes bind to derivatized CDs as selectors in gas chromatography. Their goals are to explore systematically suitable GC-compatible chiral selectors that are more universal with regard to their application. They prepared 2,3-di-O-methyl-6-O-*tert.*-butyldimethylsilyl- β -CD (TBCD) for comparison with the more common permethyl- β -CD (PMCD) CSP. The idea was to narrow the secondary opening of the cavity and block the opening on the primary side of the CSP. The TBCD was dissolved in a lipophilic polysiloxane (OV-1701) and coated on treated and non-pretreated silica capillary surfaces. The test compounds studied were limonene and 1-phenylethanol. (*S*)-limonene is eluted before the *R*-enantiomer and $\alpha = 1.078$ on TBCD and $\alpha = 1.029$ on PMCD. The *R*-enantiomer emerges before the *S*-enantiomer for the polar alcohol with $\alpha = 1.044$ on TBCD and 1.048 on PMCD.

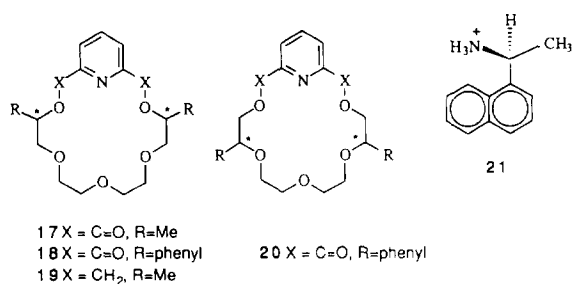
The molecular modeling involved converting

the X-ray structure of permethyl- β -CD to TBCD. The structure was energy minimized and subjected to molecular dynamics at high temperatures to probe its conformations. Likewise, the analyte conformations were probed and these conformers were placed in the interior of the CD cavity. A Monte Carlo docking algorithm was used to generate guest–host complexes which were then geometry optimized by molecular mechanics. A distance-dependent dielectric constant was used to simulate the presence of the polysiloxane matrix. In this way a range of energies for each diastereomeric complex were generated as were average energy differences that were in agreement with their experiment. Moreover, from their simulations, they were able to determine the number of inclusion complexes formed between each guest and host; the more stable complex always had the larger number of inclusion complexes. Based on their modeling studies and experimental observations, the authors drew several conclusions about how the analytes bind and fit into the TBCD cavity and the influence of CSP rigidity on chiral discrimination.

Other atomistic molecular modeling studies on molecules that serve as type III CSPs exist. The first, by Gehin et al. [45], used MM and MD to understand how *D*- and *L*-phenylglycine methyl esters bind to Cram's macrocycle. A 1.3 kcal mol⁻¹ energy difference favoring the *L*-enantiomer is in agreement with NMR studies but no chromatography on this CSP was done.

Bradshaw et al. [46] constructed new crown ethers that could serve as CSPs, tested their ability to resolve enantiomeric amines and used molecular mechanics to help understand how these potential CSPs work so that better ones could be designed. Chiral polyethers **17–20** were synthesized and their free energies of dissociation with (*R*) vs. (*S*)-1-(1-naphthyl)ethyl ammonium perchlorates (**21**) were determined by NMR methods. The computed enthalpy differences of the lowest energy *R* vs. *S* complexes did not agree very well with the experimental free energy differences, but in all cases the more tightly bound substrate was correctly predicted.

In a later study [47], other pyridine–18-crown-



6 polyethers were synthesized and their dissociation free energies with chiral alkylammonium salts were measured. The degree of chiral recognition of these chiral crown ethers is substantial. Again using MM, all of conformational space was scanned to find the lowest energy structures of the host and the chiral guest ammonium ions were complexed with these low-energy conformations. These structures were then geometry optimized. The enthalpy differences for nineteen enantiomer pairs were computed in this way. Of these, six have experimental dissociation free energies that compare fairly well with theory. Structural comparisons of the diastereomeric complexes helped elucidate how chiral recognition takes place but, because these macrocyclic hosts have yet to be implemented in chromatographic resolutions, we shall not pursue this.

Finally, we point out a paper by Alvira et al. [48] which, although not involving chromatography, should nonetheless be of interest. In this paper the authors compute the interaction between a helix and amino acids. The helix, consisting of glucose rings, is characterized by its radius, pitch and charge distribution. Intermolecular interactions are computed with a potential energy function as used in molecular mechanics. Various helix characteristics representing helicoidal polysaccharides such as cellulose or chiral cavities such as cyclodextrins were used. The chiral discrimination increases when the analyte molecule is inside the cavity formed by the helix and the chiral discrimination of D- and L-amino acids is 2-8% of the total interaction energy.

5. Type IV CSPs

These kinds of stationary phases involve solute association with a metal complex as in chiral ligand-exchange chromatography (CLEC). To our knowledge, there are no reported atomistic computations in this area but there are molecular modeling studies of chiral mobile phase additives which are coordination complexes as well as modeling in chiral ion-pair chromatography that will be discussed here.

In a recent report, Bazylak [49] compared the resolution of underivatized primary and secondary amino alcohols by reversed-phase HPLC using nickel(II) chelates as a mobile phase additive with traditional CLEC. The coordination complexes prepared are depicted in Fig. 9, where the substituents at stereocenters *z* and *q* were modified. These compounds are helically distorted nickel(II) Schiff base chelates derived from condensation of optically pure tetradentate Schiff base ligands with nickel(II) acetate. These coordination complexes work differently from ligand-exchange chelates by virtue of the fact that during association with analytes the chelate structure remains intact. In other words, no coordinating bonds between the nickel and Schiff-base ligand have been broken or formed, and the coordinatively unsaturated nickel(II) only has specific steric and electrostatic interactions with the two analytes. No energy calculations were done. Rather, least-squares superpositions of analyte with chelating reagent were depicted showing where the author believes

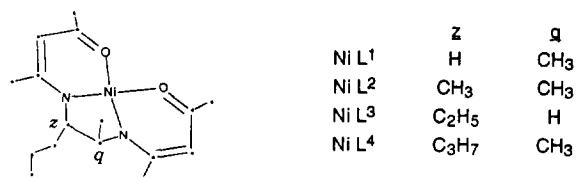


Fig. 9. Computer model of NiL₄ chelate as an example of the structure of helical nickel(II) chelates used as mobile phase additive. The asymmetric carbon atoms are designated *z* and *q*. The hydrogen atoms have been omitted for clarity.

negatively charged amine groups associate with the metal and how other interactions such as π -stacking with the chelate rings induce chiral discrimination.

Another report on ion-pair chromatography, where computed molecular descriptors from molecular modeling were nicely correlated with experimented separation factors, was published by Karlsson et al. [50]. They examined factors responsible for separation of aminotetralins **22**–**27** on achiral stationary phases in the presence of the chiral additive L-ZGP (N-benzyloxycarbonyl-glycyl-L-proline), a protected peptide derivative.

Using the MMX force field, these authors first determined the distribution of conformational states accessible to the analytes and then evaluated the preferred conformations of L-ZGP in the neutral and ionic forms. Then the authors brought these components together to form the various diastereomeric complexes. In their studies their strategy was to implement a flexible docking scheme because it was felt that both molecules of the complex may change their conformations during association.

To put this in perspective, the authors found 40 conformations with energy <3 kcal mol⁻¹ from the global minimum (the most stable conformer) for **22** and 243 low-energy conformations for L-ZGP. This would require 40×243 combinations, each one of which would have a large number of orientations and positions with respect to one another, to consider. Thus a computer-aided docking protocol was used to com-

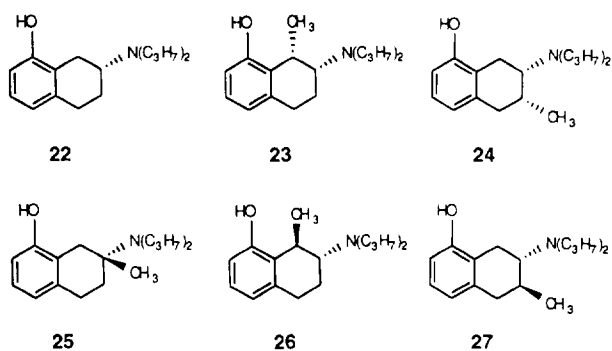
plement their manual docking results. For each diastereomeric complex, over 10^4 unique geometries were saved and subjected to molecular mechanics energy minimization which produced, in turn, about 1500 low-energy structures. Stereographic views of L-ZGP with **22**, **23** and **24** are presented in Fig. 10.

These structures are amongst thousands that can participate in the act of chiral discrimination. Accordingly, the authors decided not to use only the lowest energy structures but rather all of their data to derive averaged energies and averaged properties for comparison to experiment. The best molecular descriptor found to correlate with experiment is the averaged non-polar unsaturated surface area of the complex vs. α . A more recent paper extending their studies to include 4-hydroxy-2-dipropylaminoindan has appeared [51]. Similar conclusions were derived.

6. Type V CSPs

Type V CSPs are protein phases where analytes may adsorb from repulsive hydrophobic forces and attractive polar interactions. It would appear that, with nearly 400 entries in the Brookhaven Protein Databank to select from (X-ray and neutron data), separation scientists would have used one of these proteins to serve as a chiral selector and carry out molecular modeling studies on type V stationary phases whose structures are known. This has not happened. Rather, treating the CSP as an unknown, quantitative structure–enantioselective retention relationships (QSERRs) have been carried out.

Norinder and Hermansson [52] separated 35 N-aminoalkylsuccinimides (**28**) on an α_1 -acid glycoprotein (AGP) column. To explore the relationship between molecular structure and enantioselectivity, a principal component analysis with partial least-squares projection techniques allowed the authors to determine which of 50 physico-chemical descriptors correlated with separation factors, α . A partial list of variables used in the models is given in Table 3. Similar descriptors along with indicator variables for the other R groups on **28** give rise to the



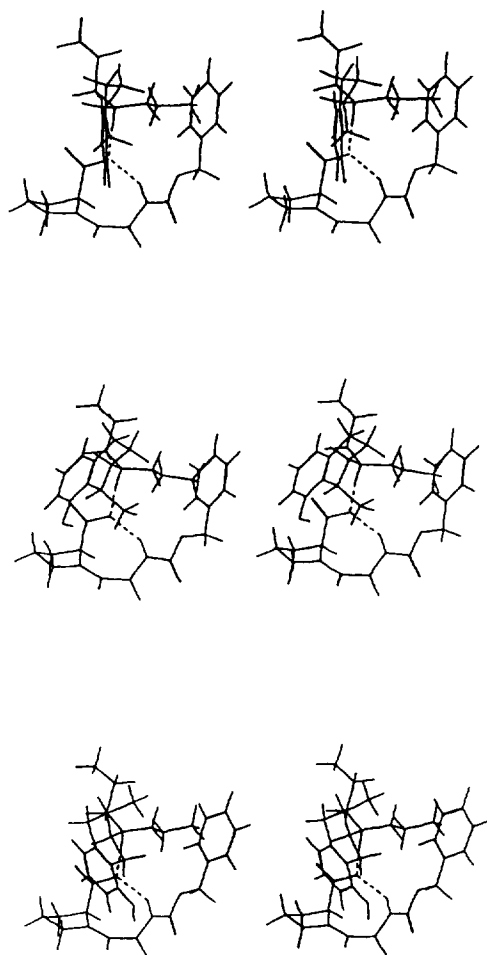


Fig. 10. Stereoscopic representation of changes in complex conformation resulting from the introduction of methyl groups in different positions of the non-aromatic ring of **22**. Energy-minimized (*R*)-**22**-L-ZGP complex (top); energy-minimized complex resulting from the introduction of a *cis*-1-methyl group forming the (*1S,2R*)-**23**-L-ZGP complex (middle); energy minimized complex resulting from introduction of a *cis*-3-methyl group forming the (*2S,3R*)-**24**-L-ZGP complex (bottom). Complexes formed by introduction of methyl groups in the *trans* C-1 and C-3 positions and in the C-2 position did not show significant changes in the complex geometries compared with (*R*)-**22**-L-ZGP.

other variables used. Some variables such as n and MR are obvious, but other terms such as the minimum width (B_1) and maximum width (B_5) should be looked up in the original literature.

Four significant principal components describing 85% of the variance were found. The most

important variables were associated with positions 6 and 7 on the aryl ring. Lipophilic groups containing aromatic character are especially important for enantioselectivity and the length of the aliphatic side chain was also found to be important.

Another QSERR was carried out by Kaliszan et al. [53], who suggested that many of the abstract and arbitrary indicator variables used by Norinder and Hermansson obscure the physical interpretation of the correlations. These authors measured the retentions of 21 chiral and achiral 1,4-benzodiazepine derivatives (**29–32**) on an immobilized human serum albumin CSP. The variables used to determine the QSERR consisted of molecular descriptors derived from computational chemistry. Regression analysis to the data resulted in equations for both enantiomers with these non-empirical molecular descriptors.

$\log k'_1$ and $\log k'_2$ were considered as two sets of mutually independent variables. The resulting models were

$$\log k'_1 = -1.75 + 0.39 \log f_y - 1.84C_3 - 0.16W + 0.04\beta_{CCN} + 0.17f_x \quad (17)$$

$$\log k'_2 = 1.99 + 0.89P_{SM} + 0.48f_y - 4.15C_3 - 0.12W + 0.13f_x \quad (18)$$

where f_y is the hydrophobicity of substituents on position 7, C_3 is the atomic charge on carbon 3 derived by semi-empirical molecular orbital calculations, W is the width of the analyte, β_{CCN} is the diazepine C-2–C-3–C-4 angle, f_x is the hydrophobicity of substituents at carbon 2' and P_{SM} is the substructure dipole which is the charge difference between the hydrogen at C-3 and the most negatively charged atom multiplied by the distance (D in Fig. 11) between them. Eqs. 17 and 18 allow one to gain an insight into the retention mechanism. Eq. 17 indicates that the binding site responsible for the first-eluted isomer contains structural and spatial constraints and that the hydrophobicity of group Y at C-7 is most important by anchoring the analyte to the CSP. Counteracting this is the excess charge at C-3 and the width of the binding site, which

Table 3
Partial list of variables used in the Norinder–Hermansson models

No.	Variable	Position	Explanation
1	n		Chain length, number of CH ₂ groups
2	n^2		Chain length, number of CH ₂ groups
3	MR	R ₁	Molecular refractivity
4	MR^2		Molecular refractivity
5	L	R ₁	Verloop Sterimol parameter
6	L^2	R ₁	Verloop Sterimol parameter
7	B_1^1	R ₁	Verloop Sterimol parameter
8	B_1^2	R ₁	Verloop Sterimol parameter
9	B_5	R ₁	Verloop Sterimol parameter
10	B^2	R ₁	Verloop Sterimol parameter
11	f	R ₁	Rekkers aliphatic fragmental constant
12	f^2	R ₁	Rekkers aliphatic fragmental constant
13	MR	R ₂	Molecular refractivity
14	MR^2	R ₂	Molecular refractivity
15	L	R ₂	Verloop Sterimol parameter
16	L^2	R ₂	Verloop Sterimol parameter
17	B_1^1	R ₂	Verloop Sterimol parameter
18	B^2	R ₂	Verloop Sterimol parameter
19	B_5	R ₂	Verloop Sterimol parameter
20	B_5	R ₂	Verloop Sterimol parameter
21	f	R ₂	Rekkers aliphatic fragmental constant
22	f^2	R ₂	Rekkers aliphatic fragmental constant

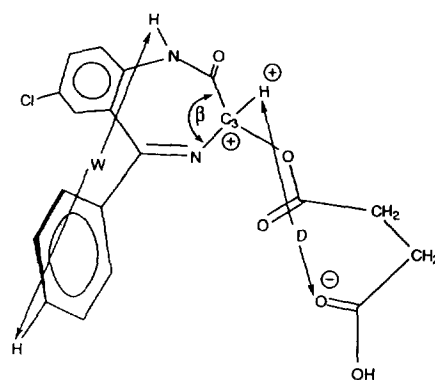
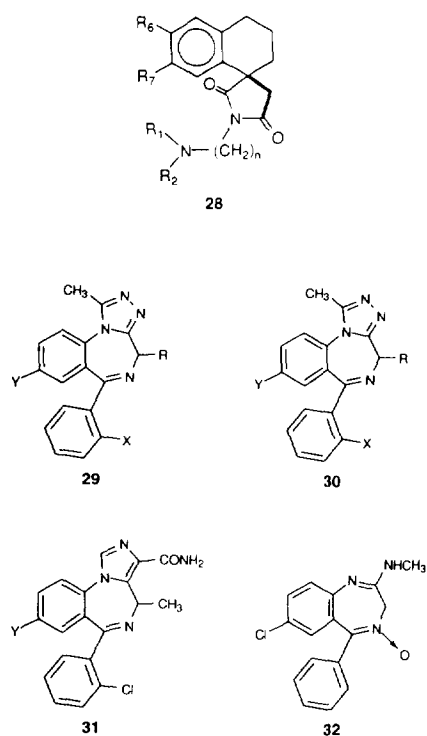


Fig. 11. Several of the molecular descriptors used in a QSERR study of 1,4-benzodiazepine analogues on a human serum albumin-based HPLC chiral stationary phase.

appears to be restricted. Eq. 18 indicates that the second-eluted isomer is influenced by the same structural features as the first-eluted enantiomer, i.e., hydrophobicity, f_y , excess charge at C-3 and width. However, the most significant retention descriptor for $\log k'_2$ is the local dipole, P_{SM} . This indicates that the greatest difference be-

tween binding sites for the enantiomers involves the charge density of the cationic area on the exterior of the CSP. The significant conclusion derived from this computational approach is that there appear to be two distinct binding sites on the protein CSP for chiral benzodiazepines.

7. Summary and conclusions

Molecular modeling studies directed toward understanding where and how chiral discrimination takes place in chromatography have been reviewed. This review focused on CSP types II–V and complements an earlier review that focused on type I CSPs [12]. In contrast to type I phases, where intermolecular interactions between selector and selectand were explicitly calculated with quantum or molecular mechanics tools, one finds more regression models for type II–V CSPs. The reason for this is that the shape of these CSPs is, with the exception of cyclodextrin and several synthetic hosts, not well defined or not known at all. Hence all one can do is rely on regression models. These models, albeit lacking a detailed atom-by-atom account of the interactions taking place during chromatography, do provide important information concerning where and how chiral recognition takes place. Moreover, these models are capable of making predictions. That is, once the model has been constructed and validated, one can use those same kinds of molecular descriptors to predict what the separation will be for an as yet unknown analyte.

It is important to realize that molecular modeling is in its infancy. The computational tools available for simulating analyte separation under a variety of chromatographic conditions with various stationary phases, chiral and achiral, gas or liquid, exist. However, we point out that while these computational tools are powerful when used properly, one still would like to use one's experience to determine how best to resolve enantiomers chromatographically. In this regard, then, we point out the enormous research effort by Roussel and Piras [54] and Koppenhoefer et al. [55], who created and

maintain CHIRBASE, a graphical molecular database on the separation of enantiomers by gas, liquid and supercritical fluid chromatographies. A more recent and potentially very useful database once it is more complete is CHIRULE, a column selection system using similarity searching, developed by Stauffer and Dessy [56]. Databases such as these together with the computational methodologies described above allow one to make a better selection of the chromatographic tools needed for a resolution and provide insights concerning the mechanism of chiral discrimination. The future of molecular modeling and computational chemistry in the separation sciences looks bright.

Acknowledgement

This work was carried out under the auspices of a grant from the Petroleum Research Fund administered by the American Chemical Society (25343-AC4) and a grant from the National Science Foundation.

References

- [1] R.W. Souter, *Chromatographic Separations of Stereoisomers*, CRC Press, Boca Raton, FL, 1985.
- [2] M. Zeif and L. Crane (Editors), *Chromatographic Chiral Separations (Chromatographic Science Series, Vol. 40)*, Marcel Dekker, New York, 1987.
- [3] W.A. Konig, *The Practice of Enantiomer Separation by Capillary Gas Chromatography*, Hüthig, Heidelberg, 1987.
- [4] S.G. Allenmark, *Chromatographic Enantioseparation. Methods and Application*, Ellis Horwood, Chichester, 1988.
- [5] D. Stevenson and I.D. Wilson (Editors), *Chiral Separations*, Plenum Press, New York, 1988.
- [6] W.J. Lough (Editor), *Chiral Liquid Chromatography*, Blackie, London, 1989.
- [7] D. Stevenson and I.D. Wilson (Editors), *Recent Advances in Chiral Separations*, Plenum Press, New York, 1990.
- [8] S. Ahuja (Editor), *Chiral Separations by Liquid Chromatography (ACS Symposium Series, No. 471)*, American Chemical Society, Washington, DC, 1991.
- [9] G. Subramanian (Editor), *Chiral Separations by Liquid Chromatography*, VCH, Weinheim 1994.

- [10] For a list of books, monographs and reviews on this topic, see the citations in H.J. Schneider, *Angew. Chem., Int. Ed. Engl.*, 30 (1991) 1417.
- [11] For a review series covering all aspects of computational chemistry, see K. Lipkowitz and D. Boyd (Editors), *Reviews in Computational Chemistry*, Vols. 1–6, VCH, New York, 1990–95.
- [12] K.B. Lipkowitz, *J. Chromatogr. A*, 666 (1994) 493.
- [13] I.W. Wainer, *Trends Anal. Chem.*, 6 (1987) 125.
- [14] S. Weinstein, L. Leiserowitz and E. Gil-Av, *J. Am. Chem. Soc.*, 102 (1980) 2768.
- [15] S. Weinstein, B. Feibush and E. Gil-Av, *J. Chromatogr.*, 126 (1975) 97.
- [16] S. Weinstein and L. Leiserowitz, *Acta Crystallogr., Sect. B*, 36 (1980) 1406.
- [17] R. Isaksson, H. Wennerstrom and O. Wennerstrom, *Tetrahedron*, 44 (1988) 1697.
- [18] R.M. Wolf, E. Francotte and D. Lohmann, *J. Chem. Soc., Perkin Trans. 2*, (1988) 893.
- [19] C. Roussel, J.-L. Stein, M. Sergent and R. Phan Tan Luu, in D. Stevenson and I.D. Wilson (Editors), *Recent Advances in Chiral Separations*, Plenum Press, New York, 1990, p. 105.
- [20] C. Roussel and C. Popescu, *Chirality*, 6 (1994) 251.
- [21] C. Roussel, S. Lehuédé, C. Popescu and J.-L. Stein, *Chirality*, 5 (1993) 207.
- [22] P. Camilleri, J.A. Murphy, M.R. Saunders and C.J. Thorpe, *J. Computer-Aided Mol. Design*, 5 (1991) 277.
- [23] I. Alkorta, J. Elguero, P. Goya and C. Roussel, *Chromatographia*, 27 (1989) 77.
- [24] E. Francotte and R.M. Wolf, *Chirality*, 3 (1991) 43.
- [25] K.B. Lipkowitz, G. Pearl and M.A. Peterson, unpublished results, 1994; R.M. Wolf, E. Francotte, L. Glaser, I. Simon and H. Scheraga, *Macromolecules*, 25 (1992) 709.
- [26] L. Cavallo, P. Corradini and M. Vacatello, *Polym. Commun.*, 30 (1989) 236.
- [27] J.G. Ning, *J. Chromatogr. A*, 659 (1994) 299.
- [28] R.D. Armstrong, T.J. Ward, N. Pattabiraman, C. Benz and D.W. Armstrong, *J. Chromatogr.*, 414 (1987) 192.
- [29] R.D. Armstrong, in W.L. Hinze and D.W. Armstrong (Editors), *Ordered Media in Chemical Separations (ACS Symposium Series, No. 342)*, American Chemical Society, Washington, DC, 1987, Ch. 16.
- [30] D.W. Armstrong, T.J. Ward, R.D. Armstrong and T.E. Beesley, *Science*, 232 (1986) 1132.
- [31] R.E. Boehm, D.E. Martire and D.W. Armstrong, *Anal. Chem.*, 60 (1988) 522.
- [32] A. Berthod, S.-C. Chang and D.W. Armstrong, *Anal. Chem.*, 64 (1992) 395.
- [33] C. Roussel and A. Favrou, *Chirality*, 5 (1993) 471.
- [34] P. Camilleri, A.J. Edwards, H.S. Rzepa and S.M. Green, *J. Chem. Soc., Chem. Commun.*, (1992) 1122.
- [35] K.B. Lipkowitz, K. Green and J.-A. Yang, *Chirality*, 4 (1992) 205.
- [36] D.W. Armstrong, X. Yang, S.M. Han and R.A. Menges, *Anal. Chem.*, 59 (1987) 2594.
- [37] K.B. Lipkowitz, S. Raghothama and J.-A. Yang, *J. Am. Chem. Soc.*, 114 (1992) 1554.
- [38] K.B. Lipkowitz, K. Green, J.-A. Yang, G. Pearl and M.A. Peterson, *Chirality*, 5 (1993) 51.
- [39] A. Berthod, W. Li and D.W. Armstrong, *Anal. Chem.*, 64 (1992) 873.
- [40] K.B. Lipkowitz, *J. Org. Chem.*, 56 (1991) 6357.
- [41] J.E.H. Köhler, M. Hohla, M. Richters and W.A. König, *Angew. Chem.*, 104 (1992) 362; *Angew. Chem., Int. Ed. Engl.*, 31 (1992) 319.
- [42] J.E.H. Köhler, M. Hohla, M. Richters and W.A. König, *Chem. Ber.*, 127 (1994) 119.
- [43] N. Koen de Vries, B. Coussens and R.J. Meier, *J. High Resolut. Chromatogr.*, 15 (1992) 499.
- [44] F. Kobor, K. Angermund and G. Schomburg, *J. High Resolut. Chromatogr.*, 16 (1993) 299.
- [45] D. Gehin, P.A. Kollman and G. Wipff, *J. Am. Chem. Soc.*, 111 (1989) 3011.
- [46] J.S. Bradshaw, R.M. Izatt, J.J. Christensen, K.E. Krakowiak, B.J. Tarbet, R.L. Bruening and S. Lifson, *J. Inclusion Phenom. Mol. Recogn.*, 7 (1989) 127.
- [47] J.S. Bradshaw, P. Huszthy, C.W. McDaniel, C.Y. Zhu, N.K. Dalley, R.M. Izatt and S. Lifson, *J. Org. Chem.*, 55 (1990) 3129.
- [48] E. Alvira, J. Breton, J. Plata and C. Girardet, *Chem. Phys.*, 155 (1991) 7.
- [49] G. Bazylak, *J. Chromatogr. A*, 665 (1994) 75 and 668 (1994) 519.
- [50] A. Karlsson, K. Luthman, C. Pettersson and U. Hacksell, *Acta Chem. Scand.*, 47 (1993) 469.
- [51] K. Luthman, A.V. Jensen, U. Hacksell, A. Karlsson and C. Pettersson, *J. Chromatogr. A*, 666 (1994) 527.
- [52] U. Norinder and J. Hermansson, *Chirality*, 3 (1991) 422.
- [53] R. Kaliszán, T.A.G. Noctor and I.W. Wainer, *Chromatographia*, 33 (1992) 546.
- [54] C. Roussel and P. Piras, *Pure Appl. Chem.*, 65 (1993) 235.
- [55] B. Koppenhoefer, A. Nothdurft, J. Pierrot-Sanders, P. Piras, C. Popescu, C. Roussel, M. Stiebler and U. Trettin, *Chirality*, 5 (1993) 213.
- [56] S.T. Stauffer and R.E. Dessy, *J. Chromatogr. Sci.*, 32 (1994) 228.